GLOBAL BIOGEOCHEMICAL CYCLES, VOL. 10, NO. 4, PAGES 693–709, DECEMBER 1996

BIOME3: An equilibrium terrestrial biosphere model based on ecophysiological constraints, resource availability, and competition among plant functional types

Alex Haxeltine and I. Colin Prentice

Global Systems Group, Department of Ecology, Lund University, Lund, Sweden

Abstract. The equilibrium terrestrial biosphere model BIOME3 simulates vegetation distribution and biogeochemistry, and couples vegetation distribution directly to biogeochemistry. Model inputs consist of latitude, soil texture class, and monthly climate (temperature, precipitation, and sunshine) data on a 0.5° grid. Ecophysiological constraints determine which plant functional types (PFTs) may potentially occur. A coupled carbon and water flux model is then used to calculate, for each PFT, the leaf area index (LAI) that maximizes net primary production (NPP), subject to the constraint that NPP must be sufficient to maintain this LAI. Competition between PFTs is simulated by using the optimal NPP of each PFT as an index of competitiveness, with additional rules to approximate the dynamic equilibrium between natural disturbance and succession driven by light competition. Model output consists of a quantitative vegetation state description in terms of the dominant PFT, secondary PFTs present, and the total LAI and NPP for the ecosystem. Canopy conductance is treated as a function of the calculated optimal photosynthetic rate and water stress. Regional evapotranspiration is calculated as a function of canopy conductance, equilibrium evapotranspiration rate, and soil moisture using a simple planetary boundary layer parameterization. This scheme results in a two-way coupling of the carbon and water fluxes through canopy conductance, allowing simulation of the response of photosynthesis, stomatal conductance, and leaf area to environmental factors including atmospheric CO_2. Comparison with the mapped distribution of global vegetation shows that the model successfully reproduces the broad-scale patterns in potential natural vegetation distribution. Comparison with NPP measurements, and with an FPAR (fractional absorbed photosynthetically active radiation) climatology based on remotely sensed greenness measurements, provides further checks on the model's internal logic. The model is envisaged as a tool for integrated analysis of the impacts of changes in climate and CO_2 on ecosystem structure and function.

1. Introduction

Prognostic models for the assessment of climate change impacts on natural ecosystems have until now fallen into two distinct classes. Biogeography models [e.g., *Woodward*, 1987; *Neilson et al.*, 1992; *Neilson*, 1995; *Neilson and Marks*, 1994; *Prentice et al.*, 1992] simulate the potential natural distribution of ecosystem types as a function of climate and soils; biogeochemistry models [e.g., *Raich et al.*, 1991; *McGuire et al.*, 1992; *Mellilo et al.*, 1993; *Parton et al.*, 1993; *Running and Coughlan*, 1988; *Running and Gower*, 1991; *Warnant et al.*, 1994; *Woodward et al.*, 1995; *Foley*, 1994] simulate biogeochemical fluxes through ecosystems given a prescribed distribution of ecosystem types. However, it is now widely acknowledged that any serious attempt to assess how global change will affect natural ecosystems must include both aspects [*VEMAP Members*, 1995]. BIOME3 represents an attempt to combine the biogeography and biogeochemistry modeling approaches within a single global framework.

Paper number 96GB02344.
0886-6236/96/96GB02344$12.00

The ecosystems of the world can be divided into a small set of biomes (structural types) each characterized by the dominance of one or more functional types of plant. Environmental conditions (both the physical environment and other competing plant types) control the geographical distribution of a dominant plant functional type (PFT). Environmental controls on the distribution of PFTs may be categorized as ecophysiological constraints, resource availability, and competition mediated by the physical environment. Ecophysiological constraints on individual PFTs, for example, cold tolerance and seasonality requirements [*Woodward*, 1987], account for the gross qualitative features of biome distribution. These constraints formed the basis of the BIOME model of *Prentice et al.* [1992]. A small set of ecophysiological constraints also forms the first stage of BIOME3. However, vegetation structure is determined not only by the types of plants present but also by the height, foliage cover, and net primary production (NPP) that they attain, and by the relative competitive performance of different types in terms of these variables [*Schulze*, 1982]. Foliage cover, often expressed as leaf area index (LAI) and NPP are constrained by resource availability (water, nutrients, CO_2, and light), and these constraints act differentially on different PFTs affecting the outcome of competition among PFTs. For example, in tropical climates the length of the dry season and total

rainfall affect the competitive balance between evergreen and drought-deciduous woody plants. In savannas, rainfall seasonality and soil texture affect the competitive balance between woody plants and grasses. In temperate climates, the length of the summer growing season and severity of the winter affect the competitive balance between evergreen and cold-deciduous trees. In grasslands, growing season temperatures and ambient CO_2 levels affect the competitive balance between C_4 and C_3 grasses. BIOME3 simulates the control of resource availability on vegetation structure by mechanistically modeling the performance of different PFTs, including simulation of LAI and NPP. Environmental mediation of the competitive balance among plants types is modeled through comparison of the NPP values simulated for different PFTs. In this way, BIOME3 is able to simulate these more quantitative aspects of ecosystem structure.

BIOME3 is a development from a simpler prototype model (BIOME2), which was fully implemented only for Australia [*Haxeltine et al.*, 1996] and the conterminous United States [*VEMAP Members*, 1995]. Both BIOME2 and BIOME3 have been designed parsimoniously in that the number of PFTs distinguished and the complexity and detail of the biogeochemical and biophysical calculations has been kept to the minimum needed to fulfil the models primary objective of simulating large-scale vegetation patterns on a mechanistic basis.

2. Model Description

The essential model logic is as follows. First, BIOME3 selects from a global set of plant functional types (PFTs) the subset which may potentially be present in a particular grid cell on the basis of a small number of ecophysiological constraints. Using a coupled carbon and water flux model and an optimization algorithm, BIOME3 then calculates the maximum sustainable leaf area index (LAI) and net primary production (NPP) for each PFT. Competition among PFTs is simulated by using the optimal NPP of each PFT as an index of competitiveness. A semi-empirical rule designed to capture the opposing effects of succession driven by light competition and natural disturbance by fire excludes grasses as a dominant PFT if soil conditions are too wet. The PFT with the highest NPP is selected as the dominant plant type, except where grasses have been excluded. Model output consists of a quantitative vegetation state description in terms of the dominant PFT, secondary PFTs present, and the total LAI and NPP for the ecosystem. This output can be classified into biome types for comparison with vegetation maps.

The model is driven by monthly climate data. Model outputs are therefore at a monthly or yearly time step. Photosynthesis and canopy conductance are calculated at a monthly time step. The water balance and phenology models, however, work on a daily time step for reasons of numerical stability. Monthly temperature and cloudiness data are interpolated linearly between midmonths to yield quasi-daily values. Values for canopy conductance are calculated daily and then averaged to produce values for averaged midmonth days Output from the water balance and phenology submodels are averaged to provide monthly average values for use by the photosynthesis and canopy conductance submodels.

2.1. Selection of Potentially Present Plant Types

Prentice et al. [1992] summarized the different cold tolerance mechanisms employed by woody plant forms and demonstrated the importance of minimum temperatures in determining the world distributions of different types of woody plants. Following *Prentice et al.* [1992], each of the values in the first data column of Table 1 represents an approximate point of failure for a different cold tolerance mechanism, based mainly on observations summarized by *Woodward* [1987]. BIOME3 controls the distribution of the plant functional types employing these different mechanisms using data on absolute minimum temperature rather that by using an approximate relationship to mean coldest-month temperatures as in the model of *Prentice et al.* [1992]. The absolute minimum temperature tolerances given in Table 1 are the same as those given in Table 2 of *Prentice et al.* [1992] except for the temperate broad-leaved evergreen plant type (as it has no direct equivalent in the work of *Prentice et al.* [1992]) for which a value was estimated from *Woodward* [1987]. Chilling requirements are minimally represented by requiring an absolute minimum temperature below 0°C for temperate and boreal PFTs (Table 1). *Prentice et al.* [1992] distinguished temperate summergreen trees from boreal summergreen trees and temperate evergreen (coniferous) trees from boreal evergreen (coniferous) trees. In BIOME3 these distinctions are made only at the mapping stage, because in principle they do not affect the deciduous/evergreen competition. Application of these temperature limits results in the selection of between one and three potentially dominant woody PFTs.

Table 1. Absolute Minimum Temperate (T_{min}) Tolerances for Each Woody Plant Type

Plant-Type	T_{min}	
	Min	Max
Tropical broad-leaved evergreen	0	
Tropical broad-leaved raingreen	0	
Temperate broad-leaved evergreen	−10	0
Temperate/boreal evergreen conifer[a]	−60	0
Temperate/boreal summergreen[b]		0

Where the table is blank a tolerance is not specified for that plant type.
[a] Needle-leaved.
[b] Broad-leaved or needle-leaved.

2.2. Coupled Carbon and Water Flux Model

Photosynthesis. Photosynthesis is calculated as a function of absorbed photosynthetically active radiation (APAR), temperature, atmospheric CO_2 concentration, day length, and canopy conductance. Calculations are made for an averaged midmonth day and multiplied by the number of days in the month. APAR is calculated from the net photosynthetically active radiation (PAR) multiplied by the fraction of incoming PAR intercepted by green vegetation (FPAR). FPAR is calculated from the projected leaf area index (LAI) using Beer's law [*Monsi and Saeki*, 1953]:

$$\mathrm{FPAR} = 1 - \exp(-k\,\mathrm{LAI}) \quad (1)$$

where k is an extinction coefficient. Measurements of k indicate that it varies considerably among different species of plant and that

Table 2. Values of Parameters and Constants Used in the Photosynthesis Model

Symbol	Value	Units	Q_{10}	Description
K_c	30[a]	Pa	2.1	Michaelis constant for CO_2
K_o	30[a]	kPa	1.2	Michaelis constant for O_2
τ	2600[b]		0.57	CO_2/O_2 specificity ratio
α_{C3}	0.08[a]			C_3 quantum efficiency
b_{C3}	0.015[c]			R_d/V_m ratio for C_3 plants
λ_{mC3}	0.7[d]			optimal c_i/c_a for C_3 plants
α_{C4}	0.053[e]			C_4 quantum efficiency
b_{C4}	0.035			R_d/V_m ratio for C_4 plants
λ_{mC4}	0.4			optimal c_i/c_a for C_4 plants
α_a	0.5			scaling parameter for α
c_a	340	µmol mol^{-1}		ambient mole fraction CO_2
P	100	kPa		atmospheric pressure
O_2	20.9	kPa		partial pressure O_2
C_{mass}	12	g mol^{-1}		molar mass of carbon
k	0.5[f]			extinction coefficient
θ	0.7[g]			co-limitation parameter

[a] *Collatz et al.* [1991].
[b] *Brooks and Farquhar* [1985].
[c] *Farquhar et al.* [1980].
[d] *Wong et al.* [1979].
[e] *Ehleringer and Björkman* [1977].
[f] *Woodward* [1987].
[g] *McMurtrie and Wang* [1993].

it is also dependant on sun angle [*Larcher*, 1983]. Here we use an average value of k (Table 2) appropriate for modeling photosynthesis at large scales [*Woodward*, 1987]. The net PAR flux is calculated from latitude, temperature, and sunshine hours data using an algorithm fully described in the appendix. Canopy conductance is calculated as a function of potential photosynthesis rate and water stress through coupling with the water flux model. Water stress is assumed to reduce photosynthesis through a reduction in canopy conductance. The mechanism of this reduction is not treated explicitly.

The photosynthesis scheme is based upon the Farquhar photosynthesis model as simplified by *Collatz et al.* [1991]. However, instead of prescribing values for the Rubisco capacity (V_m), we use an optimization algorithm to predict, for each month, the value of V_m that gives the maximum (non-water-stressed) daily rate of net photosynthesis. This algorithm is based upon very extensive evidence, summarized by *Haxeltine and Prentice* [1996], for the hypothesis that the N content and Rubisco activity of leaves vary both seasonally and with canopy position in such a way as to maximize net photosynthesis. Here leaf nitrogen content is not modeled explicitly; instead, the optimization is carried out directly on the Rubisco activity of leaves. The optimization depends on the fact that both the maximum rate of gross photosynthesis and the leaf respiration rate increase with the activity of photosynthetic enzymes (most importantly Rubisco) in the chloroplasts. This results in a trade-off: a high net photosynthesis rate at high PAR can be achieved by having a high Rubisco activity, but this also implies a low, or negative, net photosynthesis rate at low PAR. Thus, for any PAR level there is an optimal photosynthetic enzyme activity that produces maximum net photosynthesis.

The resulting scheme has the important feature that it predicts lightuse efficiencies that are independent of PAR. *Haxeltine and Prentice* [1996] showed that this scheme estimates lightuse efficiencies consistent with those measured in crop ecosystems but up to double those measured in natural ecosystems. They hypothesized that this is because lightuse efficiencies and photosynthesis rates are reduced in natural ecosystems by temperature, water, and nutrient stresses.

Here we summarize the photosynthesis scheme, for which *Haxeltine and Prentice* [1996] give a full rationale. Daily net photosynthesis is calculated using a standard nonrectangular hyperbola formulation, which gives a gradual transition between two limiting rates: J_E, describing the response of photosynthesis to APAR; and J_C, describing the Rubisco limited rate of photosynthesis [*Collatz et al.*, 1991; *Haxeltine and Prentice*, 1996]

$$A_{nd} = [J_E + J_C - \{(J_E + J_C)^2 - 4 J_E J_C\}^{1/2}] / (2\theta) - R_d \quad (2)$$

where

$$J_E = C1_{C3}\,\mathrm{APAR} \quad (3)$$

$$C1_{C3} = \Phi_c\,\Phi_{TC3}\,C_{mass}\,\alpha_a\,\alpha_{C3}\,[(p_i - \Gamma_*) / (p_i + \Gamma_*)] \quad (4)$$

$$J_C = C2_{C3}\,V_m \quad (5)$$

$$C2_{C3} = (p_i - \Gamma_*) / \{p_i + K_c(1 + [O_2] / K_o)\} \quad (6)$$

where A_{nd} is the daily net photosynthesis (g C d^{-1} m^{-2}) and R_d is the daily leaf respiration rate (g C d^{-1} m^{-2}). APAR is the daily total absorbed PAR (mol d^{-1} m^{-2}), and α_{C3} is the intrinsic quantum efficiency for CO_2 uptake as measured in laboratory studies. The empirical parameter α_a accounts for reductions in PAR utilization efficiencies in natural ecosystems, and is assigned a value of 0.5 based on data summarized by *Landsberg* [1986] on quantum efficiencies from field and laboratory measurements. C_{mass} is the molar mass of carbon, and p_i is the internal partial pressure of CO_2, given by

$$p_i = \lambda\,p_a \quad (7)$$

where p_a is the ambient partial pressure of CO_2 and λ is a parameter. Many observations have shown that, for C_3 species under non-water-stressed conditions, stomata respond in a way that maintains a constant ratio of intercellular (p_i) to ambient (p_a) CO_2 partial pressure of 0.6-0.8 [*Wong et al.*, 1979; *Long and Hutchin*, 1991]. We therefore set λ equal to a maximum value (λ_{mC3}=0.7) under non-water-stressed conditions. Γ_* is the CO_2 compensation point given by

$$\Gamma_* = [O_2] / 2\tau \quad (8)$$

where $[O_2]$ is the partial pressure of oxygen. K_c, K_o, and τ are kinetic parameters whose temperature dependence is modeled using a Q_{10} relationship. The empirical parameter θ describes the transition between the two limiting rates J_E and J_C, and may be determined experimentally. The inhibition function Φ_{TC3} models the effect of low temperatures on C_3 photosynthesis:

$$\Phi_{TC3} = \{1 + \exp[0.2\,(10 - T_c)]\}^{-1} \quad (9)$$

where T_c is the monthly temperature (in degrees Celsius). The function was adjusted so as to approximate the response of C_3 photosynthesis to low temperatures [*Berry and Björkman*, 1980]. Φ_c is a PFT specific parameter (Table 4) to account for the observation that maximum rates of photosynthesis for conifer needles decrease with increasing needle age. Leaf respiration (R_d in g C d^{-1} m^{-2}) was scaled to V_m as

$$R_d = b_{C3} V_m \tag{10}$$

where b_{C3}=0.015 [*Farquhar et al.*, 1980]. The values of all parameters and constants used in the photosynthesis model are given in Table 2.

The model calculates the value of V_m which gives the maximum daily rate of net photosynthesis. This optimal value for V_m is calculated by optimizing (2) using the constraint $\partial A_{nd}/\partial V_m$=0, resulting in the following equation for V_m (g C d^{-1} m^{-2}):

$$V_m = (1 / b_{C3}) (C1_{C3} / C2_{C3}) [(2\theta - 1)s - (2\theta s - C2_{C3})\sigma] \text{ APAR} \tag{11}$$

$$\sigma = [1 - (C2_{C3} - s) / (C2_{C3} - \theta s)]^{1/2} \tag{12}$$

$$s = (24 / d_l) b_{C3} \tag{13}$$

where d_l is the day length in hours, calculated as described in the appendix.

A model for C_4 photosynthesis was adapted from *Collatz et al.* [1992] using the same optimization procedure. For C_4 photosynthesis the functions $C1_{C3}$ and $C2_{C3}$ are replaced by $C1_{C4}$ and $C2_{C4}$ which are calculated as

$$C1_{C4} = \Phi_{pi} \Phi_{TC4} C_{mass} \alpha_a \alpha_{C4} \tag{14}$$

$$C2_{C4} = 1 \tag{15}$$

where α_{C4} is the intrinsic quantum efficiency for C_4 photosynthesis, and Φ_{pi} and Φ_{TC4} are scalars which reduce the C_4 photosynthesis rate below its optimal value. Φ_{pi} captures the effect of reduced p_i on C_4 photosynthesis:

$$\Phi_{pi} = \lambda / \lambda_{mC4} \tag{16}$$

where λ_{mC4} is the value of λ which C_4 plants maintain under non-water-stressed conditions. Φ_{TC4} accounts for the approximate response of C_4 plants to extreme temperatures, following *Collatz et al.* [1992]:

$$\Phi_{TC4} = \{1 + \exp[0.3 (13 - T_c)]\}^{-1} \{1 + \exp[0.3 (T_c - 36)]\}^{-1} \tag{17}$$

Leaf respiration costs are calculated as in (10) but with the parameter b_{C3} replaced by b_{C4}. The value of b_{C4} was scaled so as to give leaf respiration costs for C_4 photosynthesis similar to those predicted for C_3 photosynthesis. An optimal value of V_m is calculated from (11) using the appropriate functions and parameter values for C_4 photosynthesis [*Haxeltine and Prentice*, 1996]. The values of all parameters used in the C_4 photosynthesis model are listed in Table 2.

With a plentiful water supply this scheme gives C_4 photosynthesis rates that are lower than C_3 rates at temperatures <20°C; above this temperature, C_4 rates are higher. Water stress tends to have a greater effect on the modeled C_3 photosynthesis rate than on the C_4 rate; thus water stress lowers the temperature at which the C_4 photosynthesis rate exceeds the C_3 rate.

The photosynthesis rate may be related to canopy conductance through the diffusion gradient in CO_2 concentration implied by the difference in CO_2 concentration between the atmosphere and intercellular air spaces. Expressing this relationship in terms of the total daytime net photosynthesis A_{dt} gives

$$A_{dt} = [(g_c - g_{min}) / 1.6] [c_a (1 - \lambda)] \tag{18}$$

where g_c is the average daytime canopy conductance. The parameter g_{min} is a PFT specific minimum canopy conductance, which accounts for plant water loss not directly associated with photosynthesis (e.g. cuticular transpiration). The variable c_a is the ambient mole fraction of CO_2 (p_a=P×c_a, where P is atmospheric pressure). The factor of 1.6 accounts for the difference in the diffusion coefficients of CO_2 and water vapor. A_{dt} is given by

$$A_{dt} = A_{nd} + (1 - d_l / 24) R_d \tag{19}$$

Equation (18) may be rearranged to calculate a value for g_c:

$$g_c = g_{min} + 1.6 A_{dt} / [c_a (1 - \lambda)] \tag{20}$$

Use of the maximum non-water-stressed value for λ (λ_{mC3} for C_3 photosynthesis) allows the calculation of the maximum potential photosynthesis rate and maximum potential canopy conductance (g_p) realizable under non-water-stressed conditions

$$g_p = g_{min} + 1.6 A_{dt} / [c_a (1 - \lambda_{mC3})] \tag{21}$$

Water stress results in a lower canopy conductance. In which case the water balance calculation provides a value for the actual (water-limited) canopy conductance; (18) is then solved as a simultaneous equation with (2) (using a bisection method) to obtain the water-limited values of A_{nd} and λ.

Evapotranspiration. The actual evapotranspiration (AET) is calculated at a daily time step as the minimum of a supply function S and a non-water-stressed evapotranspiration rate D:

$$\text{AET} = \min\{S, D\} \tag{22}$$

D is calculated as a function of the potential canopy conductance (g_p) using a simple planetary boundary layer parameterization adapted from *Monteith* [1995]:

$$D = E_q \alpha_m [1 - \exp(-g_p / g_m)] \tag{23}$$

where E_q is the daily total equilibrium evapotranspiration calculated from latitude, temperature and sunshine hours data as described in the appendix. The parameters α_m and g_m are empirical parameters with α_m = 1.4 and g_m = 5 following *Monteith* [1995]. The variable g_p is the non-water-stressed potential canopy conductance predicted by the photosynthesis model. D gives the evapotranspiration rate which the vegetation achieves when the supply of moisture from the soil is not limiting.

Following *Prentice et al.* [1993], the supply function is proportional to the soil moisture in the rooting zone (W_r):

$$S = E_{max} W_r \tag{24}$$

where E_{max} is the maximum daily transpiration rate possible under well watered conditions, assigned a value of 5 mm d^{-1} based on

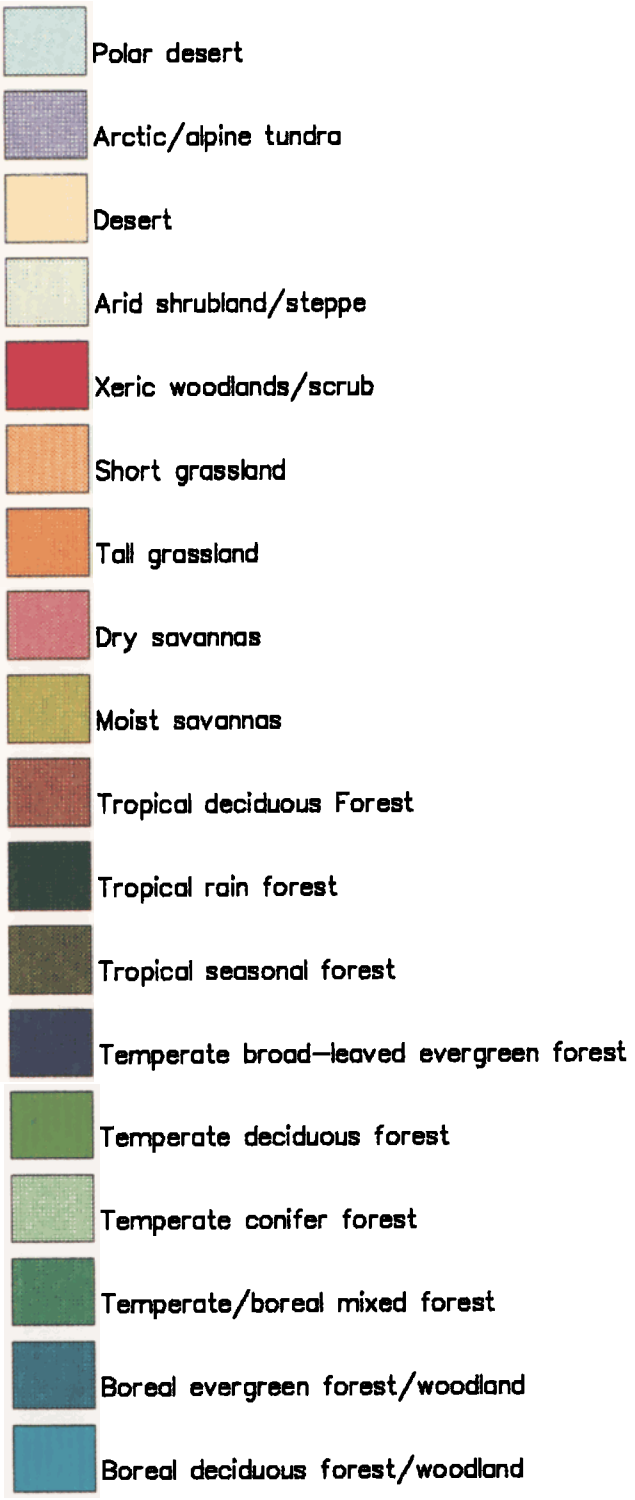

Plate 1. Legend for Plates 2 and 3.

on differences in the model's ability to predict different vegetation classes and, using a subjective scale, can be used to assess the predictive ability of the model. *Monserud* [1990] suggested that values <0.4 be considered poor or very poor, values 0.4-0.55 be considered fair, values 0 55-0 7 be considered good, values 0 7-0.85 be considered very good and values >0.85 be considered excellent. A generalized form of the kappa statistic [*Prentice et al.*, 1992] can be used in a similar way to examine the agreement between the two maps at spatial scales larger than the grid size. Adjacent grid cells are grouped into blocks and the proportions of different classes within each block are calculated. The overall agreement between maps is then based on the similarity between the proportions of different classes found within the blocks.

The overall kappa statistic reveals a fair agreement (0.53) between the maps at a 0.5° block size and a good agreement (0.58) at a larger 2.5° block size. Model predictions thus show a better agreement with the vegetation map at larger scales. This is to be expected because both the soils and vegetation data sets are largely composed of data originally digitized at a 1° resolution rather than the 0.5° resolution used for this study, and the 0.5° climate data set was produced by interpolation between climate stations with a spacing often considerably more than 0.5°. Individual kappa statistics for each biome are shown in Table 6 for block sizes of 0.5° and 2.5°. They reveal differences in the models performance for different vegetation classes.

The predicted extents of the forest and woodland classes generally show a fair to good agreement with the vegetation map. Exceptions are the temperate conifer, tropical deciduous forests, and xeric woodlands/scrub classes. The predicted distribution of temperate conifer forest is in very poor agreement with the map. The predicted extent of xeric woodlands/scrub biome shows a poor agreement with the map on the basis of the kappa statistic. However, the model correctly predicts areas of xeric woodlands/scrub in southwestern Australia, the Cape region of South Africa, the circum-Mediteranean region, central Chile, Mexico, and California. The major area of disagreement is in South America where the model predicts savannas in two large areas mapped as xeric woodlands/scrub. The predicted extent of tropical deciduous forests also show a poor agreement with the vegetation map on the basis of the kappa statistic. The transition from tropical seasonal forest to tropical deciduous forest is correctly predicted in most places. The disagreement is thus largely due to the fact that the model predicts savannas in some areas mapped as tropical deciduous forests. The predicted extent of the desert, arid shrubland, and tundra biomes all show a good agreement with the vegetation map.

Grasslands and savannas versus forests, woodlands, and shrublands. The model predicts that grasses will compete successfully against woody plant types in drier environments where summer rain favors grasses by increasing the water supply in the top soil layer and/or where conditions are warm enough and dry enough for C_4 grasses to be significantly more competitive than C_3 plants.

A test of the ability of the model to simulate the global distribution of grass versus woody plant types was made by aggregating the vegetation classes (Table 7). The overall kappa statistic thus obtained of 0.61 at a 0.5° block size and 0.65 at a 2.5° block size indicates the success of the model in predicting the dominance of grasslands and savannas versus woodlands and forests at the global scale.

The kappa statistics obtained for grasslands and savannas with the full set of vegetation classes show only a poor agreement (Table 6) between the simulated and mapped vegetation. This suggests that the model is less successful at differentiating moist

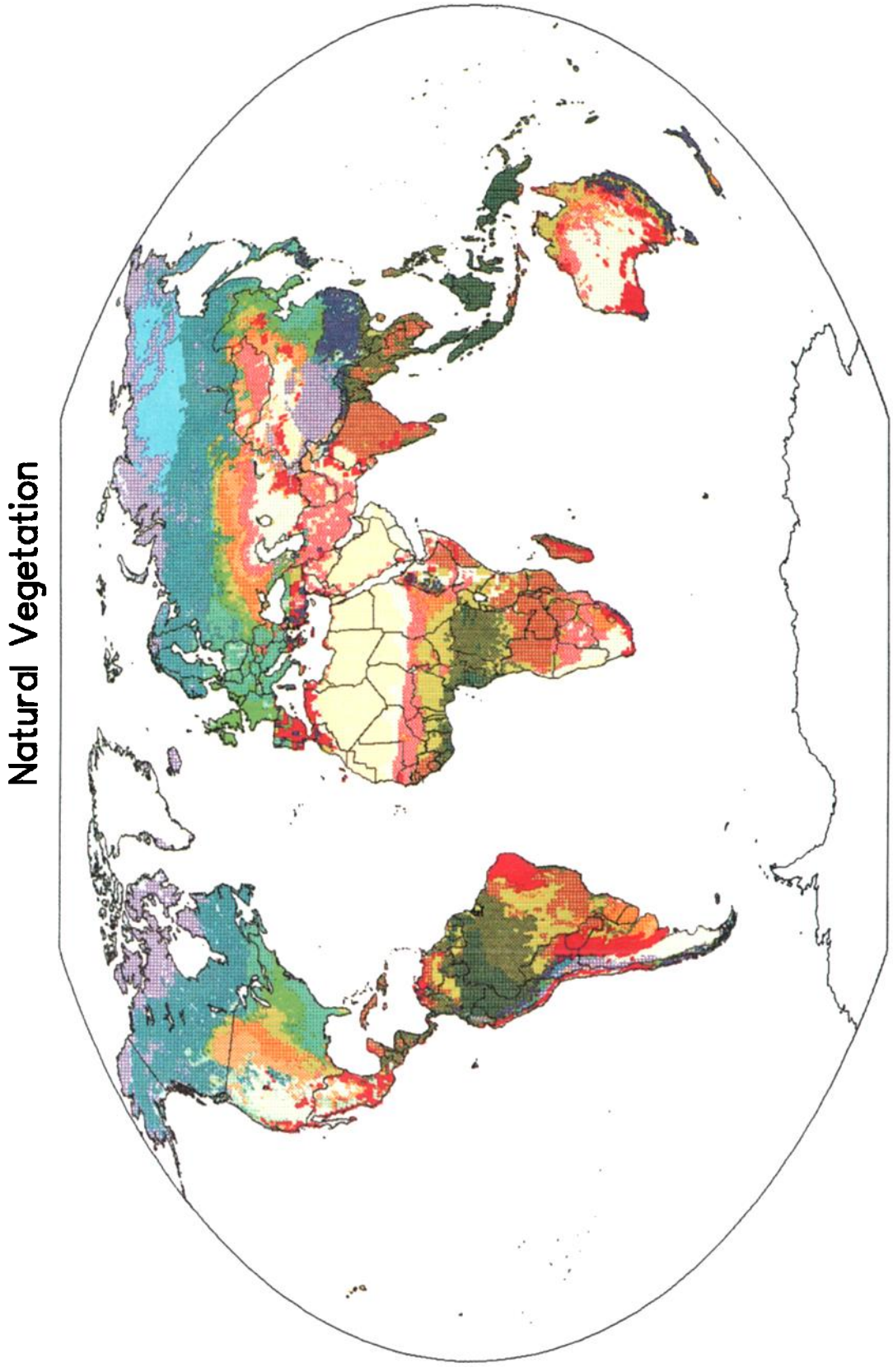

Plate 2. Potential natural vegetation map for comparison with Plate 3.

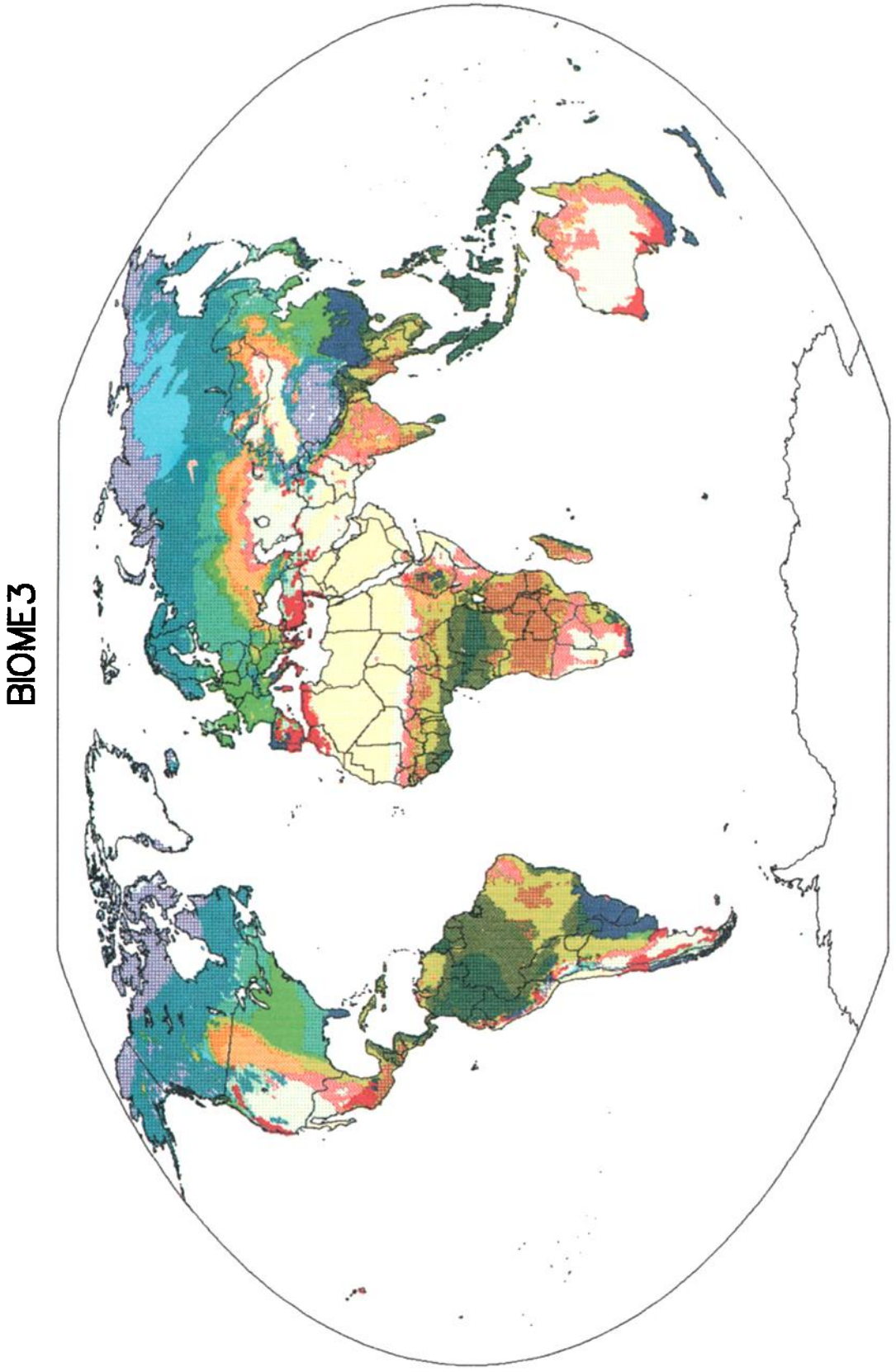

Plate 3. Simulated vegetation distribution.

data summarized in *Kelliher et al.* [1993]. The supply function empirically captures (based on observation) the reduction in transpiration which occurs because of decreases in canopy conductance related to decreasing soil moisture.

Canopy conductance. If the water supply is not limiting, the actual canopy conductance (g_c) is equal to the maximum potential canopy conductance (g_p). If the actual evapotranspiration rate is limited by soil moisture (i.e., if S<D), a water-limited canopy conductance is calculated as the canopy conductance implied by the actual (supply-limited) evapotranspiration rate:

$$g_c = g_p \qquad S > D$$
$$g_c = -g_m \ln[1 - S/(E_q \alpha_m)] \qquad S < D \tag{25}$$

g_c is then used to calculate the actual (water-limited) photosynthesis rate. The resulting values for canopy conductance (g_c) depend mainly upon environmental conditions and photosynthetic pathway (only the minimum canopy conductance is directly plant-type specific). The maximum potential canopy conductance (g_p) is linearly related to the maximum daily photosynthesis rate, as in (21). Thus, under conditions of limited water stress, the model predicts a linear relationship between the maximum canopy conductance and the maximum photosynthesis rate in agreement with observation [*Schulze et al.*, 1994].

The calculation is complicated by the fact that evapotranspiration is calculated at a daily time step, while photosynthesis is calculated at a monthly time step. Values for g_p are estimated by the photosynthesis model for twelve midmonth days and then linearly interpolated to provide daily values for the evapotranspiration calculation. These values of g_c are used to calculate the actual photosynthesis for an averaged midmonth day and then multiplied by the number of days in the month.

Soil hydrology. The soil is described by two layers at depths 0–500 mm and 500–1500 mm. Available water holding capacity (AWC, in millimetres) for each layer is defined as the difference between field capacity and wilting point for the relevant soil texture. Monthly rainfall totals are linearly interpolated to yield quasi-daily rainfall values. The soil moisture stores are updated each day using the daily percolation (Perc, in millimetres) , quasi-daily rainfall (Rain, in millimetres), snowmelt (Melt, in millimetres) and the calculated evapotranspiration rate (AET, in millimetres):

$$\Delta W_1 = (Melt + Rain - Perc - \beta_1 AET)/AWC_1 \tag{26}$$

$$\Delta W_2 = (Perc - \beta_2 AET)/AWC_2 \tag{27}$$

$$\beta_1 = Z W_1 / W_r \tag{28}$$

$$\beta_2 = (1 - Z) W_2 / W_r \tag{29}$$

$$W_r = [Z W_1 + (1 - Z) W_2] \tag{30}$$

where W_1 and W_2 are the soil water contents for the previous day (expressed as a fraction of the AWC in that layer); ΔW_1 and ΔW_2 are the daily changes in W_1 and W_2, respectively. AWC_1 and AWC_2 are the available water holding capacities of the upper and lower soil layers, respectively. The parameters β_1 and β_2 give the rates of extraction of transpired water from the upper and lower soil layers, respectively (such that $\beta_1+\beta_2=1$). Z is a PFT specific parameter defining the fraction of the plants roots which are in the top soil layer. W_r is the average soil moisture in the rooting zone.

Percolation from the upper layer to the lower layer is calculated using an empirical equation adapted from *Neilson* [1995]. The percolation formula is:

$$Perc = K W_1^4 \tag{31}$$

where *Perc* is the daily percolation (in millimetres) from the upper to the lower soil layer, K is an empirical parameter (in millimetres) dependent on soil texture, and W_1 is the fractional wetness of the upper soil layer (as a fraction of the AWC). The equation is an empirical analog of Darcy's Law [*Neilson*, 1995] with conductivity being represented as a power function of soil wetness (K gives the percolation rate when soil moisture in the upper soil layer is at field capacity). Percolation depends on soil texture through the value of K. Runoff occurs from the upper layer when the upper layer reaches field capacity and from the lower layer when the lower layer reaches field capacity.

Daily precipitation is defined as rain or snow depending on temperature being above or below –2°C. Snow melt is driven by temperature scaled by a melt coefficient:

$$Melt = (T_d - 2) S_m \tag{32}$$

where T_d is the quasi-daily temperature and $S_m = 0.7$ mm $^{\circ}C^{-1}$ d^{-1}. No snowmelt is allowed when the snowpack is depleted.

Soil moisture on day one is estimated by initializing the soil moisture stores at a value scaled to annual rainfall and then running the water flux and phenology models for an initial spin-up year. Soil moisture values predicted for the last day of this spin-up year are then used for initializing a final run.

Values for the soil-texture dependent parameters are given in Table 3. The parameter K was calibrated so as to give magnitudes and ranges of percolation consistent with the four basic soil texture classes. AWC for each layer was calculated as the product of the volumetric water holding capacity (H_{max}) and the depth of the soil layer. Values for H_{max} were calculated following the method described by *Prentice et al.* [1992]. The soil hydrology and evapotranspiration schemes have been extensively tested against high-

Table 3. Soil-Texture Dependant Parameters

Texture-Type	H_{max}, %	K, mm d^{-1}
Vertisols	10.0	0.2
Fine	12.0	3.0
Medium	15.0	4.0
Coarse	11.0	5.0
Medium-coarse	13.0	4.5
Fine-coarse	11.5	4.0
Fine-medium	13.5	3.5
Fine-medium-coarse	12.7	4.0
Organic	30.0	9.0

H_{max} is the volumetric water holding capacity at field capacity minus the volumetric water holding capacity at wilting point; K is an empirical parameter in the percolation equation.

quality soil hydrological and micrometeorological data during a recent workshop on soil moisture simulation [*Shao et al.*, 1994].

Respiration costs. Whole plant respiration is calculated at a yearly time step as

$$R_{total} = R_{leaf} + R_{transport} + R_{fine\_root} + R_{growth} \quad (33)$$

where R_{total} is the total annual plant respiration costs, R_{leaf} is annual leaf respiration, $R_{transport}$ is annual maintenance respiration costs for transport tissues (e.g., stem and woody root sapwood), R_{fine_root} is fine root respiration, and R_{growth} is annual growth respiration.

Leaf respiration costs are calculated at a monthly time step by the photosynthesis model and summed to obtain R_{leaf}.

Maintenance respiration for transport tissues is modeled as a function of the estimated total carbon content (C_s) of transport tissues. C_s is estimated as a simple function of leaf area index (LAI) following the "pipe model" theory of plant form [*Shinozaki et al.*, 1964]:

$$C_s = \text{LAI}\, C_n \quad (34)$$

where C_s is the total sapwood carbon content (kg C m^{-2}), LAI is the leaf area index, and C_n is a parameter for the sapwood carbon content per unit LAI (kg C m^{-2}). An average value for C_n was estimated by combining estimates of the proportion of biomass in sapwood [*Ryan*, 1989; *Rogers and Hinckley*, 1979] with estimates of average standing biomass from *Olson et al.* [1983] and *Larcher* [1983], resulting in the value of C_n being set equal to 1 kg C m^{-2}. A modified Arrhenius relationship is used for the dependence of transport tissue maintenance respiration on temperature, following *Lloyd and Taylor* [1994]:

$$R_{transport} = \sum_{m=1}^{m=12} K_r C_s \exp[\, E_o f(T_c)\,] \quad (35)$$

$$f(T_c) = (T_{ref} - T_o)^{-1} - (T_c - T_o)^{-1} \quad (36)$$

where m is the number of the month and T_c is the mean monthly temperature (in degrees celcius), K_r is the sapwood respiration rate (g C kg^{-1} C $month^{-1}$) at the reference temperature (T_{ref}) of 10°C, E_o=308.56 K, and T_o=–46.02°C. A mean value for K_r of 1.67 g C kg^{-1} C $month^{-1}$ was estimated from data presented in Table 2A of *Sprugel et al.* [1996].

Raich and Nadelhoffer [1989] presented data, from a wide range of forest ecosystems in different climate zones, that showed a strong correlation between total belowground carbon allocation (B_a) and total annual leaf litterfall carbon (L_f). They derived an equation for total annual below ground carbon allocation, $B_a = 130 + 1.92\, L_f$. However, the intercept was not significantly different from zero. We make the assumption that when averaged across all vegetation types, B_a will tend to zero as L_f tends to zero, implying that $B_a/L_f \approx 2$. Furthermore, fine root construction and maintenance respiration are thought to account for about half of B_a [*Sprugel et al.*, 1996; *Ryan*, 1991; *Runyon et al.*, 1994] leading to the simple approximation

$$R_{fine\_root} = a\, L_f \quad (37)$$

where a=1. Leaf litterfall can be calculated from LAI, specific leaf area (SLA), and leaf longevity. Data presented by *Reich et al.* [1992] show that SLA decreases with leaf longevity in such a way as to keep litterfall approximately constant across the continuum from short-lived deciduous leaves to long-lived evergreen leaves, suggesting a simple relationship between litterfall and LAI:

$$L_f = \text{LAI}\, L_n \quad (38)$$

where LAI is the leaf area index and L_n is the total annual leaf litterfall per unit leaf area. The value of L_n was estimated as 50 g C m^{-2} from relationships given by *Reich et al.* [1992]. Growth respiration (R_{growth}) is estimated as 20% of the gross photosynthate remaining after all other respiration costs have been removed [*Ryan*, 1991].

2.3. Plant Functional Types

Just five woody and two grass plant functional types (PFTs) are used in the model. Differences in physiology, phenology and rooting depth between the PFTs result in differences in their performance in the carbon and water flux model.

Rooting Depth. Grass roots are assumed to extract water almost entirely from the upper soil. Woody plants extract water from both the upper and lower soil layers (Table 4). The rooting depth parameters follow *Haxeltine et al.* [1996].

Table 4. Plant-Type Specific Parameters Used in the Model

Plant-Type	*P*	*Z*	C_4	Φ_c	g_{min}
Tropical broad-leaved evergreen	E	0.33	no	1	0.5
Tropical broad-leaved raingreen	R	0.33	no	1	0.5
Temperate broad-leaved evergreen	E	0.33	no	1	0.5
Temperate/boreal conifer	E	0.33	no	0.8	0.3
Temperate/boreal summergreen	S	0.33	no	1	0.5
Cool grass	S	0.90	yes	1	0.5
Warm grass	E	0.90	yes	1	0.8

P: phenological type where E is evergreen, S is summergreen, R is raingreen. Z, fraction of roots in the upper soil layer. C_4 indicates whether plant-type may use C_4 photosynthetic pathway. The parameter Φ_c defines the fractional reduction in photosynthesis in conifers due to leaf age. The parameter g_{min} is the minimum canopy conductance in millimeters per second.

Photosynthesis Rates for Evergreen Conifers. Evergreen needle-leaved conifers are assigned lower rates of photosynthesis (Table 4) , based on the observation that photosynthetic rates decrease with increasing needle age [*Chabot and Hicks*, 1982; *Reich et al.*, 1992]. Maximum photosynthetic rates for evergreen conifers typically decline at 30-50% per year [*Chabot and Hicks*, 1982]. However, older needles tend to occupy lower light environments in the interior of the canopy [*Schulze et al.*, 1977], so the decrease in maximum photosynthetic rate with age at the needle level results in a much smaller decrease in whole-canopy photosynthesis [*Chabot and Hicks*, 1982]. We assume, however, that this phenomenon is not solely due to needles adapting to increased shading and that it is partly due to specific characteristics of evergreen conifer needles, possibly related to winter survival adaptations. Thus the implicit assumption is made that evergreen conifers have a mean needle age >1 year, whereas deciduous trees have a mean leaf/needle age ≤1 year.

Minimum Conductances. A lower value of the minimum canopy conductance is assigned to conifer plant types than to broad-leaved plant types (Table 4) based on observations summarized by *Körner* [1994]. Similarly, the warm grass plant is assigned a higher value of minimum stomatal conductance.

Phenology. Each PFT was assigned to be evergreen, summergreen, or raingreen (Table 4). For evergreen PFTs, leaf area is assumed constant through the year. For summergreen PFTs, leaf growth starts when the temperature rises above 5°C and takes a specified number of growing degree-days on a 5°C base (GDD, defined as $GDD=\sum(T_d-T_{oo})$, where T_d is mean daily temperature, T_{oo} is the minimum temperature for growth, and summation is over the number of days in the year with $T_d>T_{oo}$) to reach the maximum growing season leaf area (200 GDDs for summergreen woody PFTs, and 50 GDDs for the summergreen grass PFT). For raingreen PFTs a phenology algorithm was produced by calibrating soil moisture thresholds against observed raingreen phenologies: leaf area is reduced to zero whenever the soil moisture (W_r) in the rooting zone falls below 20% of the AWC in the rooting zone and is increased stepwise to the prescribed value when W_r rises above 30% of AWC in the rooting zone.

This simple phenology algorithm allows deciduous plant types to adopt an evergreen growth form under certain climates (i.e., summergreen trees growing in a climate with no monthly temperature below 5°C or raingreen trees growing in an environment with no dry period). In climates where this occurs, the deciduous plant type is allowed to be present but not dominant.

The cool grass plant type with its summergreen phenology is assigned if the temperature of the coldest month is below 5°C, otherwise the warm grass plant type with its evergreen phenology and slightly higher minimum canopy conductance is assigned.

Selection of C_4 Versus C_3 Grasses. Grasses may utilize either the C_3 or C_4 photosynthetic pathway, whereas woody plant types always use the C_3 photosynthetic pathway (Table 4) . C_4 grasses may have a lower canopy conductance and/or a higher photosynthesis rate than C_3 grasses. Both of these effects can give the C_4 grass a competitive advantage. Furthermore, the benefits incurred through having a lower canopy conductance depend upon the moisture supply over the entire growing season. Thus both temperature and moisture stress will influence the relative competitiveness of C_4 versus C_3 grasses.

In the model, the choice of a C_4 or C_3 grass type is made on a monthly basis thus allowing seasonal changes in the dominance of C_4 or C_3 grasses. The model simulates the competitive balance between C_4 and C_3 grasses under conditions of moderate water stress, as found in most grassland ecosystems. Where water is limiting, the water use efficiency (defined as net photosynthesis/transpiration) gives a better measure of the realizable photosynthesis rate than the non-water-stressed photosynthesis rate; and thus the water use efficiency more nearly defines competitive ability than the non-water-stressed photosynthesis rate. Conceptually, the model selects the grass type which can achieve the highest monthly water use efficiency as dominant. C_4 grasses are selected when the monthly temperature is sufficient for C_4 grasses to have a higher rate of photosynthesis than C_3 grasses under the constraint of a normalized transpiration rate (defined by setting λ=0.4 for both plant types). For an ambient CO_2 concentration of 340 μmol mol^{-1}, the model predicts a transition in the dominant grass type from C_3 to C_4 grasses at a monthly mean temperature (T_{C4}) of 15°C.

Ambient CO_2 concentration also influences the competitive balance between C_4 and C_3 plants. As CO_2 concentration increases, the photosynthesis rate of C_3 plants increases relative to C_4 plants; the temperature (T_{C4}) at which there is crossover from C_3 to C_4 grasses thus increases with CO_2 concentration. Furthermore, the photosynthesis model predicts a near linear increase in T_{C4} with increasing CO_2 concentration. Using the photosynthesis model to calculate T_{C4} at a range of ambient CO_2 concentrations, we developed the following regression equation for the calculation of T_{C4} at different CO_2 concentrations:

$$T_{C4} = 8 + 7\,(c_a / 340) \tag{39}$$

where c_a is the ambient CO_2 mole fraction (μmol mol^{-1}).

2.4. Prediction of Equilibrium Leaf Area and NPP

Fundamental to BIOME3 is the method used to calculate leaf area as a function of moisture and carbon limitations. *Haxeltine et al.* [1996] reviewed several approaches that have been used for estimating large-scale patterns of sustainable leaf area as a function of soil moisture availability. They showed that the simulation of maximum sustainable leaf area in water-limited environments involves capturing the balance between two opposing effects. First, water-limited vegetation will tend to support as large a leaf area as water supply allows. Second, high transpiration rates due to excessive leaf area will ultimately reduce biomass production and impair plant vigor. The problem of estimating leaf area can therefore be regarded as an optimization problem in which the benefits of increasing leaf area in terms of light interception are traded off against the costs in terms of transpiration. *Haxeltine et al.* [1996] suggested that these benefits and costs may be expressed through NPP and that the optimization described above is conceptually equivalent to maximizing NPP with respect to leaf area. The increasing costs of leaf respiration as leaf area increases are also included in the optimization of NPP.

However, the NPP obtained at a certain leaf area must also be sufficient to satisfy allocation requirements. This additional constraint is important in environments where NPP and leaf area are limited by factors other than the water supply. In such environments, such as high-latitude ecosystems, leaf area may instead be limited by an inability to satisfy whole-plant carbon allocation requirements at high leaf areas. We use the annual leaf litterfall L_f as an estimate of the absolute minimum allocation requirement. If at

a certain leaf area NPP<L_f, the leaf area is considered unsupportable and is not allowed. Then, in the absence of water limitations, the equilibrium leaf area of the vegetation is the highest leaf area for which this minimum allocation requirement is still satisfied.

On the basis of this logic the model calculates an optimal NPP and leaf area for each PFT that may potentially be present in a certain grid square. This is done by calculating NPP at a comprehensive range of leaf areas. The leaf area which gives the highest NPP, while still satisfying the minimum allocation constraint, is selected as being the optimal leaf area for that particular PFT in that grid square.

2.5. Simulation of the Dominant Plant Type

Selection of dominant PFTs is carried out using the NPP of one PFT relative to the NPP of another PFT as an index of the relative competitive ability of these two PFTs. This is done by first selecting a dominant woody PFT and then dealing with competition between the dominant woody PFT and grass PFT. The dominant woody PFT is selected from those potentially present in the grid square by selecting the woody PFT with the highest predicted NPP.

The competitive balance between woody plants and grasses in a savanna ecosystem is primarily determined by competition for available soil water [*Walter*, 1971; *Walker and Noy-Meir*, 1982; *Knoop and Walker*, 1985; *Eagleson and Segarra*, 1985; *Neilson*, 1995; *Haxeltine et al.*, 1996]. Important modifying factors are differences in physiology, fire disturbance, and competition for light [*Daubenmire*, 1978; *Walter*, 1979; *Walker and Noy-Meir*, 1982; *Hopkins*, 1992; *Neilson*, 1995]. The simulated NPP values capture the effects of competition for water resources and differences in physiology but not light competition or fire disturbance.

In moist environments, trees will tend to form a closed canopy which excludes grasses through light competition. Furthermore, fire frequency tends to be lower in moist environments than in dry environments, and frequent fires tend to favor the dominance of grasses. Through both of these mechanisms, moist environments tend to favor woody plants to the exclusion of a significant grass cover. Fire and light competition are not mechanistically modeled in BIOME3. Instead, these effects are empirically modeled by excluding grasses if the annual average available soil moisture predicted for the dominant woody PFT is >75% (where 0% available soil moisture is at the wilting point and 100% is at field capacity) or if the annual rainfall is >2200 mm. If grasses are not excluded on the basis of this moisture rule, the PFT with the highest NPP is predicted to be dominant. The competition algorithm is used to distinguish between environments in which woody plants are dominant (where woody NPP > grass NPP) versus environments in which either a grassland or savanna is the dominant vegetation type (where grass NPP > woody NPP) . In either case the modeled vegetation characteristics for the PFT with the highest NPP are assumed to be representative of the vegetation as a whole. In a earlier version of this model [*Haxeltine et al.*, 1996], competition was handled by directly simulating the performance of different combinations of grass and woody plant types. The simplification made here is to simulate the competition between grasses and woody plants by comparing the performance of a grass and woody plant type growing separately. This simplification was found to give very similar results while saving dramatically on computational costs.

2.6. Mapping to Biomes

BIOME3 predicts the NPP, the LAI, the dominant PFT, and any secondary PFTs for each grid cell. This basic model output and a number of subsidiary variables are then used to assign a biome type according to the classification scheme shown in Table 5.

3. Environmental Data Sets

3.1. Climate and Soils

Monthly mean temperature, precipitation, and percent of possible sunshine hours data were obtained from the Cramer and Leemans climate database (W. Cramer, personal communication, 1995) which is an improved version of that described by *Leemans and Cramer* [1991].

Worldwide data on absolute minimum temperatures for approximately 1000 stations were obtained from *Müller* [1982]. In this data set, absolute minimum temperature is the lowest temperature measured with a standard thermometer during the entire observation period. Differences between the absolute minimum temperatures and temperature of the coldest month were interpolated onto the 0.5° grid. Because of the relatively small number of data points for the absolute minimum temperature, the interpolation presented problems in areas where the data coverage was particularly sparse or where there was a strong spatial variation.

A soil-texture data set was constructed based on the textural information digitized by *Zobler* [1986] from the Food and Agriculture Organization soils map [*Food and Agriculture Organization*, 1974]. The data set distinguishes fine-, medium-, and coarse-textured soils and combinations of these classes, with a separate category for organic soils. In addition, we defined an extra category for vertisols. This soil type was defined for grid cells mapped as having both fine-textured soils and chromic vertisols by *Zobler* [1986].

3.2. Vegetation Data

A global map of potential natural vegetation was constructed (Plate 1) based primarily on a "hybrid" vegetation map developed by *Mellilo et al.* [1993]. The Mellilo map was constructed from a number of global and regional vegetation maps including the *Mathews* [1983], *Olson et al.* [1983], *Isachencko et al.* [1990], and *Kuchler* [1964] vegetation maps. Using the Mellilo map as a basis, further modifications were derived from the maps of *Mathews* [1983], *Olson et al.* [1983], *Isachencko et al.* [1990], and *Kuchler* [1964]. No single map contained all of the information required for a map comparison with the model output; the aim was thus to produce a vegetation map which contained the maximum amount of information for use in comparing with the model output.

The Mellilo map was used as the basis for our vegetation map, except for Africa where we used primarily the Mathews map. Areas shown in the Mellilo map to be tropical evergreen forest or tropical savanna were reclassified as tropical evergreen forest or tropical savannas according to the Mathews map. The Olson map was then used to separate tropical rain forest, tropical seasonal forest, tropical dry forest, and savannas in areas mapped by Mathews as tropical rain forest. In both tropical and temperate regions, areas of moist and dry savanna were distinguished following the Mathews and Olson maps. A distinction was made

Table 5. Classification Scheme Used to Map Model Output to Biomes

Biome Type	Dominant PFT	Leaf Area Index
Boreal deciduous forest/woodland	BTS[a]	> 0
Boreal evergreen forest/woodland	BTC[b]	> 0
Temperate/boreal mixed forest	BTS[c]	>1.5
	BTC[d]	>2.5
Temperate conifer forest	BTC[b]	>2.5 or 1.5[e]
Temperate deciduous forest	BTS[a]	> 2.5
Temperate broad-leaved evergreen forest	TBE	> 3
Tropical seasonal forest	TE	> 2.5
Tropical rain forest	TE[f]	> 2.5
Tropical deciduous forest	TR	> 2.5
Moist savannas	CG or WG	>1.5
Dry savannas	CG or WG	>0.6
Tall grassland	CG[g]	>3
	WG[h]	>3
Short grassland	CG[g]	>0.4
	WG[h]	>0.4
Xeric woodland/scrub	TBE or TR or TE	>1
	BTC or BTS	>1.5
Arid shrubland/steppe	any	>0.2
Desert	any	<0.2
Arctic/alpine tundra	any[i]	any
Polar desert	any[j]	any

The plant functional types (PFTs) are tropical broad-leaved evergreen (TE), tropical broad-leaved raingreen (TR), temperate broad-leaved evergreen (TBE), boreal/temperate summergreen (BTS), boreal/temperate evergreen conifer (BTC), cool grass (CG), and warm grass (WG). In addition to information on the dominant PFT, other potentially present PFTs, and the total LAI the classification scheme uses the following subsidiary variables: annual average available soil moisture expressed as a percentage, SM (where 0% is at the wilting point and 100% is at field capacity); monthly average available soil moisture, SM_m; temperature of the coldest month, T_{cm}; growing degree-days on 5°C base, GDD_5; growing degree-days on a 0°C base, GDD_o (GDD, defined as GDD=$\sum(T_d-T_{oo})$ where T_d is mean daily temperature, T_{oo} is the minimum temperature for growth and summation is over the number of days in the year with $T_d > T_{oo}$). Following *Prentice et al.* [1992] the temperate/boreal summergreen plant type is assigned to be boreal if T_{min}<–45°C and/or GDD_5<1200, otherwise, it is assigned to be temperate. Similarly, following *Prentice et al.* [1992], the temperate/boreal evergreen conifer plant type is assigned to be boreal if T_{min}<–45°C and/or GDD_5<1200. Otherwise, if T_{co}>–2°C, it is assigned to be temperate, and if T_{cm}<–2°C, it assigned to be a codominant mixture of both boreal and temperate types.

[a] Boreal deciduous forest is mapped if the BTS plant type is assigned to be boreal; otherwise, a temperate deciduous forest is mapped.

[b] Boreal conifer forest is mapped if the BTC plant type is assigned to be boreal; otherwise, a temperate conifer forest is mapped.

[c] Temperate/boreal mixed forest is a mapped if the BTC plant type is present and assigned to be at least partly boreal and SM>80% and NPP<600 g C m^{-2} yr^{-1}; otherwise, a deciduous forest biome is mapped.

[d] Temperate/boreal mixed forest is mapped if the BTC plant type is assigned to be temperate and the BTS plant type is also present, and SM>80%, otherwise, a deciduous forest biome is mapped.

[e] If the BTC plant type is assigned to be solely temperate, the LAI threshold of 1.5 is used, otherwise, the LAI threshold of 2.5 is used.

[f] Tropical rain forest is mapped for this PFT if SM_m>50% for all 12 months of the year; otherwise, it is mapped as tropical seasonal forest.

[g] Grassland is mapped for the cool grass plant type if SM<65% and LAI>1.5; otherwise, a savanna biome is mapped.

[h] Grassland is mapped for the warm grass plant type if the ratio of grass NPP/woody NPP >1.8; otherwise, a savanna is mapped.

[i] Tundra is always mapped if GDD_5<350, except where the requirement for polar desert is satisfied.

[j] Polar desert is always mapped if GDD_o<150.

between polar desert and tundra rather the the moist tundra and polar desert/alpine tundra classes used in the Mellilo map, again following the Mathews and Olson maps. In the circum-Mediterranean region some areas mapped as temperate savanna in the Mellilo map were reclassified as xeric woodlands/scrub, following Mathews. *Isachencko et al.* [1990] was used to map the boreal deciduous (*Larix*) woodlands in Siberia. Following *Kuchler* [1964], an area of xeric woodland/scrub was mapped in California where the Mellilo map shows temperate broad-leaved evergreen forest. The resulting natural vegetation map (see Plates 1 and 2) is derived only from vegetation data and is not in anyway derived from climate data or the output of any model.

4. Results

4.1. Comparison to Potential Natural Vegetation Map

The simulated vegetation (Plate 3) and natural vegetation map (Plate 2) were compared numerically using the kappa statistic [*Prentice et al.*, 1992]. The kappa statistic provides information

Table 6. Kappa Statistics for a Global Comparison of Simulated Vegetation Patterns With the Map of Natural Vegetation

Vegetation Class	Block Size 0.5°	2.5°
Boreal deciduous forest/woodland	0.70	0.73
Boreal conifer forest/woodland	0.68	0.70
Temperate/boreal mixed forest	0.43	0.49
Temperate conifer forest	0.15	0.28
Temperate deciduous forest	0.40	0.49
Temperate broad-leaved evergreen forest	0.43	0.52
Tropical seasonal forest	0.54	0.56
Tropical rain forest	0.70	0.69
Tropical deciduous forest	0.35	0.35
Moist savannas	0.31	0.39
Dry savannas	0.25	0.33
Tall grassland	0.25	0.31
Short grassland	0.39	0.47
Xeric woodlands/scrub	0.26	0.36
Arid shrubland/steppe	0.56	0.62
Desert	0.84	0.83
Artic/alpine tundra	0.72	0.75
Polar desert	0.42	0.58

versus dry savannas and tall versus short grasslands and/or that these distinctions are not made accurately in the vegetation map.

The model correctly predicts the temperate steppes of America and Asia. The main discrepancies are the failure of the model to predict the "Prairie Peninsula" region of the midcontinental United States and the steppe of northern Mongolian. An earlier regional version of this model [*VEMAP Members*, 1995] accurately simulated the Prairie Peninsula. For this regional application of the model a higher quality soils data set was available which resolved the soils of the Prairie Peninsula, and this is a possible reason for the discrepancy. However, the Prairie Peninsula forms a sensitive transition zone between the eastern forests and the prairie [*Daubenmire*, 1978], and the model has difficulty in resolving this transition zone. The region coincides with areas having a higher proportion of summer rainfall, and a higher interannual rainfall variability, than neighboring forests [*Neilson*, 1995]. BIOME3 is capable of predicting a savanna rather than a forest because of the influence of summer rainfall, so it is possible that consideration of the interannual variability of rainfall may be important for the accurate simulation of the Prairie Peninsula.

In South America the model fails to predict the grasslands of eastern Argentina and Uruguay. The model does not predict grassland in these areas because the precipitation is sufficiently high to support a closed forest. Other biogeography models [e.g., *Prentice et al.*, 1992; *Neilson and Marks*, 1994] also predict forest biomes in these grassland areas of South America. The cause of this discrepancy is not clear, but it may be connected with the occurrence of special soil conditions (e.g., extensive iron pans) which favor the presence of grasslands. Alternatively, the presence of grasslands in this region may be connected with the occurrence of very high rates of evapotranspiration [*Walter*, 1979] that are not fully captured in current models.

The model correctly predicts the transition from tropical seasonal forest to savanna which occurs north of the equator in Africa and the belt of moist savanna which occurs between the tropical seasonal and the tropical deciduous forest areas south of the equator in Africa. The transition from tropical seasonal forest to moist savanna occurring in areas of South America is also correctly predicted.

In Australia the model correctly predicts the pattern of xeric woodland and shrubland in the winter rain region of southwestern Australia versus the savanna and grassland of the summer rain region of northern and northeastern Australia.

The model incorrectly predicts savannas in areas of southeast Asia and India. This discrepancy occurs mostly in areas with a large but highly monsoonal rainfall. In such climates the water balance model predicts very high runoff in the monsoon months and very low soil moisture values during the dry period. The simulation of low soil moisture values results in the prediction of savanna rather than forest. In reality, a proportion of the modeled runoff would occur as base flow and be stored as ground water. Some of which would be available to the vegetation later in the year. The use of a more comprehensive hydrology model, which incorporated ground water storage, might thus allow the model to predict forests in these areas.

Cold-deciduous versus evergreen trees. The model predicts a cold-deciduous forest biome through two different mechanisms. First, in areas with absolute minimum temperatures <–60°C, the model predicts that the only trees present are boreal summergreen trees. Through this mechanism the model correctly predicts the dominance of boreal summergreen trees (*Larix* forest and woodland) in large areas of eastern Siberia.

Second, the model predicts that summergreen trees will be dominant in areas where they are able to achieve a higher carbon gain than evergreen trees. In the model, evergreen trees can achieve a higher carbon balance than summergreen trees only if their carbon gain during the part of the year when summergreen trees are without leaves outweighs the disadvantage incurred through their lower intrinsic rate of photosynthesis. Through this mechanism the model correctly predicts the major regions of tem-

Table 7. Kappa Statistics for a Global Comparison of Simulated Vegetation Patterns With the Map of Natural Vegetation Using the Reduced set of Vegetation Classes

Vegetation Class	Block Size 0.5°	2.5°
Forest/woodland	0.62	0.67
Grassland/savanna	0.45	0.50
Arid shrubland/steppe	0.56	0.62
Desert	0.84	0.83
Tundra	0.72	0.75
Polar desert	0.42	0.58

perate deciduous forest in eastern North America, Europe, and northern China.

Drought-deciduous versus evergreen tress. Drought-deciduous trees reduce carbon losses during a dry period by dropping their leaves. In the model, this allows them to outcompete evergreen trees in areas with a sufficiently long dry period. Through this mechanism the model correctly predicts the areas of tropical rain forest and seasonal forest in Amazonia and equatorial Africa versus the areas of drought-deciduous forest in southern Africa, southern Brazil, northern Australia, and Burma.

4.2. Comparison to NPP Data

A comparison was made between predicted NPP and a set of NPP field measurements (Figure 1) . There are many problems associated with such comparisons including the quality of the data and the fact that the model is simulating the average NPP over a 0.5° grid square while NPP measurements are made at particular sites. Despite these problems the resulting comparison shows a fair agreement between the predicted NPP and measurements with a linear regression (Figure 1) yielding a correlation coefficient of 0.74 (N=61 and P<0.001). A clear discrepancy is that for higher NPP sites the model tends to predict NPP values that are considerably lower than the measured values. The same effect has been observed for a number of other global NPP models [*Moore et al.*, 1995] when compared to these NPP measurements (D. W. Kicklighter, personal communication, 1995), suggesting that the higher NPP measurements may not always be representative of the average NPP in the area surrounding the measurement site.

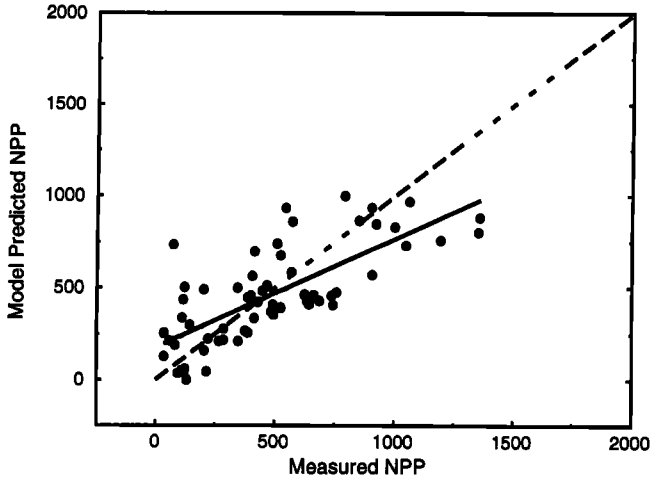

Figure 1. Comparison between BIOME3 predicted annual net primary production (NPP) and NPP field measurements. The NPP data [*Leith and Whittaker*, 1975] is the same as was used for the calibration and validation of the Terrestrial Ecosystem Model [*Raich et al.*, 1991; *McGuire et al.*, 1992; *Melillo et al.*, 1993]. NPP measurements were compared to the predicted NPP for the 0.5° grid square within which each measurement site was located. Where more than one measurement fell within one 0.5° grid square, the measurements were averaged to produce one value for the whole grid square. The solid line shows a linear regression of predicted NPP against measurements, and the dashed line indicates exact agreement.

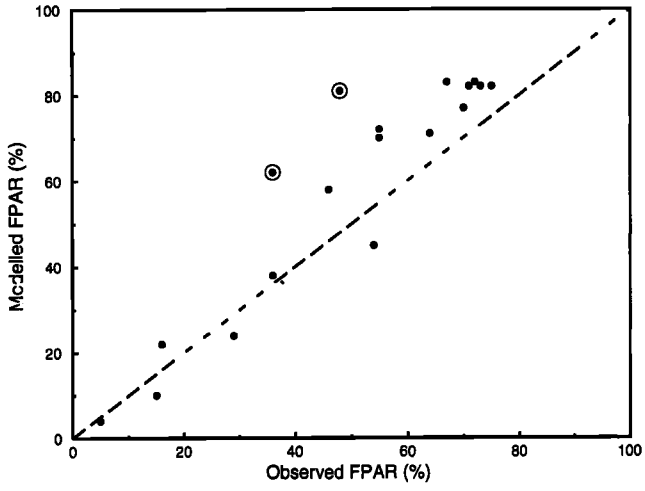

Figure 2. Comparison of biome-averaged values of predicted maximum monthly FPAR versus values obtained from remote sensing data [*Sellers et al.*, 1994, 1996]. Values for the tall and short grassland biomes are circled.

4.3. Comparison to Remote Sensing Derived FPAR Data

FPAR (the fraction of incoming photosynthetically active radiation intercepted by green vegetation) is an important ecosystem variable fundamental to the prediction of photosynthesis and NPP. Modeled FPAR values depend solely on modeled LAI values (see (1)), so that maximum monthly FPAR values are directly related to the predicted growing-season LAI.

A global FPAR data set at 1° resolution was obtained for the years 1987-1988 from the ISLSCP CD-ROM [*Sellers et al.*, 1994, 1996]. Monthly values were averaged for the 2 years. Maximum monthly FPAR values were then obtained from the averaged data set. An obvious limitation of comparing the predicted versus observed FPAR values is that the model predicts FPAR values for potential natural vegetation, whereas the observed FPAR values are influenced by agriculture and land use change. Another limitation is that the period of satellite observations is different from and much shorter than the period of climatological observation used to drive the model.

With these caveats in mind, a global comparison was made between the observed maximum monthly FPAR values and the BIOME3 predictions of maximum monthly FPAR. A linear regression (at a 1° resolution) of predicted versus observed maximum monthly FPAR values yields a correlation coefficient of 0.76 (N=14441, P<0.001, slope=0.86, and intercept=0.135) indicating a good global agreement. A comparison of the biome-averaged values of predicted versus observed maximum monthly FPAR (Figure 2) shows this agreement. The two biomes showing the least agreement with observations are tall and short grassland (Figure 2) . The model may be overpredicting LAI and thus FPAR for C_4 grasses; on the other hand, a large part of the area predicted by BIOME3 to be grassland is now, in fact, agricultural land (e.g., the Great Plains region of the United States), and this may be a primary cause of the disagreement.

5. Discussion

BIOME3 represents an attempt to model the global distribution of potential natural vegetation types by interactively coupling structure and function. Modeled vegetation distribution is partially determined by modeled NPP, while vegetation type in turn affects NPP. Using this novel design, the model successfully reproduces the broad-scale patterns in potential natural vegetation for the current climate. It also produces estimates of NPP and leaf area that are in reasonable agreement with the currently available validation data.

BIOME3 does not explicitly model the nitrogen cycle. NPP and leaf area are thus never constrained by nutrient availability in the model. Yet the model predicts reasonable values of leaf area and NPP for high-latitude ecosystems, where NPP and leaf area are known to be nutrient-limited [*McGuire et al.*, 1992]. The model succeeds because these high-latitude ecosystems are predicted to be carbon-limited. It seems likely that in the steady state, carbon and nitrogen tend to become co-limiting in high-latitude ecosystems. This has also been proposed in a recent modeling study [*Schimel et al.*, 1995] which showed that productivity has a feedback on nitrogen availability: higher productivity leads to more nitrogen being captured in biomass and subsequently soil carbon. As N retention increases, N availability tends to increase leading to a correlation of nutrient availability with other limitations on productivity. BIOME3 is thus apparently able to capture the equilibrium response of vegetation to climate without explicitly modeling the nitrogen cycle. However, when vegetation is forced away from equilibrium by rapid climate change, the carbon-nitrogen-water linkages are likely to induce a series of important feedbacks, whose accurate representation would require explicit modeling of the nitrogen cycle.

Fire and other natural disturbance regimes are not mechanistically incorporated in BIOME3. Fire frequency is an important modifying factor in determining the competitive balance between grass and woody plant types [*Daubenmire*, 1978; *Hopkins*, 1992]; in BIOME3 the dynamic equilibrium between succession-driven light competition (favoring trees) and disturbance by fire (favoring grasses) is represented by empirical rules based on moisture conditions. Again, it seems likely that such rules can describe the steady state conditions, but to simulate transient responses (to climate change, human effects on fire frequency, and their interaction), it will be necessary to take account of the specific mechanisms involved.

An important potential application of BIOME3 is for simulating the equilibrium response of vegetation to changed climates and atmospheric CO_2 concentrations. BIOME3 can simulate the changes in vegetation distribution, NPP, and leaf area resulting from a changed climate. In addition, the model captures the direct responses of photosynthesis and stomatal conductance to changes in CO_2 and simulates the effects of this response on leaf area, NPP, and the dominant plant types. The model is thus able to mechanistically simulate the direct effect of changing CO_2 on vegetation distribution, leaf area, and NPP.

BIOME3 simulates the vegetation distribution that is in equilibrium with a particular climate and atmospheric CO_2 concentration. Equilibrium vegetation models have already proved to be useful for studying the response of vegetation to palaeoclimates, and BIOME3 will add to this work by allowing quantification of the relative importance of changes in atmospheric CO_2 concentration to changes in paleovegetation distribution. For prediction of the response of vegetation to a future rapidly changing climate, BIOME3 is able suggest the general direction and maximum extent of change to be expected. Prediction of the transient response of vegetation to climate change will require the addition of a scheme to simulate vegetation dynamics and natural disturbance. By providing a means to estimate the potential distribution and productivity of different PFTs, BIOME3 represents a major step toward the development of an integrated dynamic model of the terrestrial biosphere.

Appendix: Calculation of Net Photosynthetically Active Radiation, Net Radiation, and Equilibrium Evapotranspiration

Daily net photosynthetically active radiation (PAR) is calculated in units of mol $m^{-2}d^{-1}$ as

$$PAR = (0.5 / e^*) R_s \tag{A1}$$

where R_s is the daily net short wave radiation flux in MJ d^{-1} and e* converts to molar units with e* = 0.27 MJ mol^{-1}. This assumes that 50% of the daily net short wave radiation flux is PAR. The daily net radiation is the daily net downward short wave flux R_s minus the daily net upward long wave flux R_l:

$$R_n = R_s - R_l \tag{A2}$$

Following *Linacre* [1968] and *Prentice et al.* [1993], we take

$$R_s = zz\,(c + d\,n_i)\,(1 - \beta)\,Q_o \tag{A3}$$

where c and d are empirical constants (c=0.25 and d=0.50). *Friend* [1996] calculated the values of c and d used here from a regression of the ratio of measured to potential radiation versus the percentage of maximum possible sunshine hours for a set of 161 stations from the Müller [1982] climate data set. The variable n_i is the proportion of possible hours of bright sunshine, β is the shortwave albedo set to equal to an average value of 0.17 following *Prentice et al.* [1993],

$$Q_o = 3600\,Q_{oo}\,[1 + 2 \times 0.01675 \cos(360\,i / 365)] \tag{A4}$$

where Q_{oo} is the solar constant (1360 W m-2) and i is the day number (from 1-365 starting at January 1), and

$$zz = u\,h + v\,(24 / 2\pi) \sin(360\,h / 24) \tag{A5}$$

where

$$u = \sin(l) \sin(aa) \tag{A6}$$

$$v = \cos(l) \cos(aa) \tag{A7}$$

where l is latitude,

$$aa = -23.4^\circ \cos[360\,(i + 10) / 365] \tag{A8}$$

and h is the day length in hours, calculated as

$$\begin{aligned} h &= 0 && u \le v \\ h &= 24\,[\mathrm{acos}(-u / v) / 2\pi] && u > -v,\ u < v \\ h &= 24 && u \ge v \end{aligned} \tag{A9}$$

The daytime net upward longwave flux can be approximated by a linear function of temperature over a limited range of absolute temperatures that occur near the Earth's surface [*Monteith*, 1973]. Again, following *Linacre* [1968] and *Prentice et al.* [1993]

$$S_l = h\,3600\,[b + (1-b)n_i]\,(A - T_d) \qquad \text{(A10)}$$

where b and A are empirical constants (b=0.2 and A=107 Wm^{-2}) and T_d is the mean daily temperature (°C).

Following *Jarvis and MacNaughton* [1986], the daily equilibrium evapotranspiration rate (E_q) is given by

$$E_q = [ss / (ss + \gamma)]\, R_n / L \qquad \text{(A11)}$$

where R_n is the daily total net radiation flux (J m^{-2} d^{-1}) and ss is the rate of increase of saturated vapor pressure with temperature (Pa K^{-1}), given by

$$ss = 2.5\times10^6 \exp[17.269\,T_d / (237.3 + T_d)] / (237.3 + T_d)^2 \qquad \text{(A12)}$$

where γ is the psychrometer constant, approximately 65 Pa K^{-1} and L is the latent heat of vaporization of water, approximately 2.5 $\times 10^6$ J kg^{-1}. Tables are used to take account of the weak dependence of γ and L on temperature.

Acknowledgments. This work was supported by the Swedish Natural Science Research Council (NFR) through a doctoral fellowship to A.H. for the project "Simulation Modeling of Global Vegetation Change". This is a contribution to the core research of the IGBP project on Global Change and Terrestrial Ecosystems (GCTE).

References

Berry, J.A., and O. Björkman, Photosynthetic temperature response and adaptation to temperature in higher plants, *Ann. Rev. Plant Phys.*, *31*, 491-543, 1980.

Brooks, A., and G.D. Farquhar, Effects of temperature on the CO_2/O_2 specificity of ribulose-1,5 bisphosphate carboxylase/oxygenase and the rate of respiration in the light, *Planta*, *165*, 397-406, 1985.

Chabot, B.F., and D.J. Hicks, The ecology of leaf life spans, *Ann. Rev. Ecol. Syst.*, *13*, 229-259, 1982.

Collatz, G.J., J.T. Ball, C. Grivet, and J.A. Berry, Physiological and environmental regulation of stomatal conductance, photosynthesis and transpiration: A model that includes a laminar boundary layer, *Agric. For. Meteorol.*, *54*, 107-136, 1991.

Collatz, G.J., M. Ribas-Carbo, and J.A. Berry, Coupled photosynthesis-stomatal conductance model for leaves of C_4 plants, *Aust. J. Plant Physiol.*, *19*, 519-538, 1992.

Daubenmire, R., *Plant Geography*, Academic, San Diego, Calif., 1978.

Eagleson, P.S., and R.I. Segarra, Water-limited equilibrium of savanna vegetation systems, *Water Resour. Res.*, *21*, 1483-1493, 1985.

Ehleringer, J., and O. Björkman, Quantum yields for CO_2 uptake in C_3 and C_4 plants, *Plant Physiol.*, *59*, 86-90, 1977.

Food and Agriculture Organization, *Soil Map of the World* 1:5,000,000, U.N. Educ., Sci., and Cult. Organ., Paris, 1974.

Farquhar, G.D., S. von Caemmerer, and J.A. Berry, A biochemical model of photosynthetic CO_2 assimilation in leaves of C_3 plants, *Planta*, *149*, 78-90, 1980.

Foley, J.A., Net primary productivity in the terrestrial biosphere: The application of a global model, *J. Geophys. Res.*, *99*(D10), 20773-20783, 1994.

Friend, A.D., Parameterization of a global daily weather generator for terrestrial ecosystem and biogeochemical modeling, *Ecol. Model.*, in press, 1996.

Haxeltine, A., and I.C. Prentice, A general model for the Light-use efficiency of primary production, *Funct. Ecol.*, in press, 1996.

Haxeltine, A., I.C. Prentice, and I.D. Cresswell, A coupled carbon and water flux model to predict vegetation structure, *J. Veg. Sci.*, in press, 1996.

Hopkins, B., Ecological processes at the forest-savanna boundary, in *Nature and Dynamics of Forest-Savanna Boundaries*, edited by P.A. Furley, J. Proctor and J.A. Ratter, pp. 21-33, Chapman and Hall, New York, 1992.

Isachencko, T.I. et al., *Map of vegetation in the USSR*, Inst. Geog. of the Siberian Dep. of U.S.S.R. Acad. of Sci., Inst. Bot. of U.S.S.R. Acad. of Sci. and Moscow State Univ. Geog. Dep., Minsk, Russia, 1990.

Jarvis, P.G., and K.G. MacNaughton, Stomatol control of transpiration: scaling up from leaf to region, *Adv. Ecol. Res.*, *15*, 1-49, 1986.

Kelliher, F.M., R. Leuning, and E.-D. Schulze, Evaporation and canopy characteristics of coniferous forests and grasslands, *Oecologia*, *95*, 153-163, 1993.

Knoop, W.J., and B.H. Walker, Interactions of woody and herbaceous vegetation in a southern African savanna, *J. Ecol.*, *73*, 235-253, 1985.

Körner, C., Leaf diffusive conductances in the major vegetation types of the globe, in *Ecophysiology of Photosynthesis, Ecol, Stud.* vol. 100, edited by E.-D. Schulze and M.M. Caldwell, pp. 463-490, Springer-verlag, New York, 1994.

Kuchler, A.W., *Potential Natural Vegetation of the Conterminous United States*, Am. Geogr. Soc., New York, 1964.

Landsberg, J.J., *Physiological Ecology of Forest Production*, Academic, San Diego, Calif., 1986.

Larcher, W., *Physiological Plant Ecology*, 2nd ed., Springer-Verlag, New York, 1983.

Leemans, R., and W. Cramer, The IIASA climate database for mean monthly values of temperature, precipitation and cloudiness on a terrestrial grid, Int. Inst. Appl. Syst. Anal., RR, 91-18, 1991.

Leith, H., and R.H. Whittaker, *Primary Productivity of the Biosphere*, Springer-Verlag, New York, 1975.

Linacre, E.T., Estimating the net-radiation flux, *Agric. For. Meteorol.*, *5*, 49-63. 1968.

Lloyd, J., and J.A. Taylor, On the temperature dependence of soil respiration, *Funct. Ecol.*, *8*, 315-323, 1994.

Long, S.P., and P.R. Hutchin, Primary productivity in grasslands and coniferous forests with climate change: An overview, *Ecol. Appl.*, *12*, 139-156, 1991.

Mathews, E. J., Global vegetation and land use: New high resolution data bases for climate studies, *J. Clim. Appl. Meteorol.*, 22, 474-487, 1983.

McGuire, A.D., J.M. Mellilo, L.A. Joyce, D.W. Kicklighter, A.L. Grace, B. Moore III, and C.J. Vorosmarty, Interactions between carbon and nitrogen dynamics in estimating net primary productivity for potential vegetation in North America, *Global Biogeochem. Cycles*, *6*(2), 101-124, 1992.

McMurtrie, R.E., and Y.-P. Wang, Mathematical models of the photosynthetic response of tree stands to rising CO_2 concentrations and temperatures, *Plant Cell Environ.*, *16*, 1-13, 1993.

Melillo, J.M., A.D. McGuire, D.W. Kicklighter, B. Moore III, C.J. Vorosmarty, and A.L. Schloss, Global climate change and terrestrial net primary production, *Nature*, *363*, 234-240, 1993.

Monserud, R.A. Methods for comparing global vegetation maps. *WP-90-40*, Int. Inst. Appl. Syst. Anal., Laxenburg, Austria, 1990.

Monsi, M., and T. Saeki, Uber den Lichtfaktor in den Pflanzengesellschaften und seine Bedeutung fur die Stoffproduktion, *Jpn. J. Bot.*, *14*, 22-52, 1953.

Monteith, J.L., *Principles of Environmental Physics*, Edward Arnold, London, 1973.

Monteith, J.L., Accommodation between transpiring vegetation and the convective boundary layer, *J. Hydrol.*, *166*, 251-263, 1995.

Moore, B., III, W. Cramer, I. Rasool, D. Sahagian, W. Steffen, and the Participants in "POTSDAM 95", Global net primary productivity: Results of the Potsdam '95 IGBP NPP Model intercomparison workshop (GAIM-DIS-GTCE) - Potsdam, Germany, June 20-22, 1995, poster presented at First GAIM Science Conference, Int. Geosphere-Biosphere Programme/Global Anal., Interpret. and Model., Garmisch-Partenkirchen, Germany, September, 25-29, 1995.

Müller, J.M., *Selected Climatic Data for a Global Set of Standard Stations for Vegetation Science*, Dr. W. Junk, Norwell, Mass., 1982.

Neilson, R.P., A model for predicting continental scale vegetation distribution and water balance, *Ecol. Appl.*, *5*, 362-386, 1995.

Neilson, R.P., and D. Marks, A global perspective of regional vegetation and hydrologic sensitivities from climate change, *J. Veg. Sci.*, *5*, 715-730, 1994.

Neilson, R.P., G.A. King, and G. Koerper, Towards a rule-based biome model, *Land. Ecol.*, *7*(1), 27-43, 1992.

Olson, J.S., J.A. Watts, and L.J. Allison, Carbon in live vegetation of major world ecosystems, *ORNL-5862*, Oak Ridge Nat. Lab., Oak Ridge, Tenn., 1983.

Parton, W.J., et al., Observations and modeling of biomass and soil organic matter dynamics for the grassland biome worldwide, *Global Biogeochem. Cycles*, *7*(4), 785-809, 1993.

Prentice, I.C., W. Cramer, S. Harrison, R. Leemans, R.A. Monserud, and A.M. Solomon, A global biome model based on plant physiology and dominance, soil properties and climate, *J. Biogeogr.*, *19*, 117-134, 1992.

Prentice, I.C., M.T. Sykes, and W. Cramer, A simulation model for the transient effects of climate change on forest landscapes, *Ecol. Model.*, *65*, 51-70, 1993.

Raich, J.W., and K.J. Nadelhoffer, Belowground carbon allocation in forest ecosystems: Global trends, *Ecology*, *70*, 1346-1354, 1989.

Raich, J.W., E.B. Rastetter, J.M. Melillo, D.W. Kicklighter, P.A. Steudler, B.J. Peterson, A.L. Grace, B. Moore III, and C.J. Vörösmarty, Potential net primary productivity in South America: Application of a global model, *Ecol. Appl.*, *1*, 399-429, 1991.

Reich, P.B., M.B. Walters, and D.S. Ellsworth, Leaf life-span in relation to leaf, plant, and stand characteristics among diverse ecosystems, *Ecol. Monogr.*, *62*(3), 365-392, 1992.

Rogers, R., and T.M. Hinckley, Foliar weight and area related to current sapwood in oak, *For. Sci.*, *25*, 298-303, 1979.

Running, S.W., and J.C. Coughlan, A general model of forest ecosystem processes for regional applications, I, Hydrologic balance, canopy gas exchange and primary production processes, *Ecol. Modell.*, *42*, 125-154, 1988.

Running, S.W., and S.T. Gower, FOREST-BGC, a general model of forest ecosystem processes for regional applications, II, Dynamic carbon allocation and nitrogen budgets, *Tree Physiol.*, *9*, 147-160, 1991.

Runyon, J., R.H. Waring, S.N. Goward, and J.M. Welles, Environmental Limits on Net Primary Production and light-use efficiency across the Oregon transect, *Ecol. Appl.*, *4*, 226-237, 1994.

Ryan, M.G., Sapwood volume for three subalpine conifers: predictive equations and ecological implications, *Can. J. For. Res.*, *19*, 1397-1401, 1989.

Ryan, M.G., Effects of climate change on plant respiration, *Ecol. Appl.*, *1*, 157-167, 1991.

Schimel, D.S., B.H. Braswell, and B. Moore III, Nutrient regulation of the carbon cycle, paper presented at First GAIM Science Conference, Int. Geosphere-Biosphere Programme/Global Anal., Interpret. and Model., Garmisch-Partenkirchen, Germany, September, 25-29, 1995.

Schulze, E.-D., Plant life-forms and their carbon water and nutrient relations, in *Encyclopedia of Plant Physiology*, vol 12B, pp. 615-676, Springer-Verlag, New York, 1982.

Schulze, E. D., M. Fuchs, and M.I. Fuchs, Spatial distribution of photosynthetic capacity and performance in a mountain spruce forest of northern Germany. III. The significance of the evergreen habit, *Oecologia*, *30*, 329-348, 1977.

Schulze, E.-D., F.M. Kelliher, C. Körner, J. Lloyd, and R. Leuning, Relationships among maximum stomatal conductance, ecosystem surface conductance, carbon assimilation rate, and plant nitrogen nutrition: A global ecology scaling exercise, *Annu. Rev. Ecol. Syst.*, *25*, 629-660, 1994.

Sellers, P. J., S.O. Los, C.J. Tucker, C.O. Justice, D.A. Dazlich, G.J. Collatz, and R.A. Randall, A global 1 by 1 degree NDVI data set for climate studies, 2, The generation of global fields of terrestrial biophysical parameters from the NDVI, *Int. J. Remote Sens.*, *15*(17), 3519-3545, 1994.

Sellers, P.J., S.O. Los, C.J. Tucker, C.O. Justice, D.A. Dazlich, G.J. Collatz, and R.A. Randall, A revised land surface parameterization (SiB2) for atmospheric GCMs, 2, The generation of global fields of terrestrial biophysical parameters from satellite data, *J. Clim.*, in press, 1996.

Shao, Y., et al., Soil Moisture Simulation: A report of the RICE and PILPS workshop, *Rep. 14*, 1789 pp., Global Energ. and water Exper. Proj. Off., Sydney, Australia, 1994.

Shinozaki, K., K. Yoda, K. Hozumi, and T. Kira, A quantitative analysis of plant form - The pipe model theory, I, Basic analysis, *Jpn. J. Ecol.*, *14*, 133-139, 1964.

Sprugel, D.G., M.G. Ryan, J. Renée Brooks, K.A. Vogt, and T.A. Martin, Respiration from the organ level to the stand, in *Physiological Ecology of Coniferous Forests*, edited by W.K. Smith and T.M. Hinckley, in press, 1996.

VEMAP Members, Vegetation/Ecosystem Mapping and Analysis Project (VEMAP): A comparison of biogeography and biogeochemistry models in the context of global change, *Global Biogeochem. Cycles*, *9*(4), 407-437, 1995.

Walker, B.H., and I. Noy-Meir, Aspects of stability and resilience of savanna ecosystems, in *Ecology of Tropical Savannas*, edited by B. Huntley, pp. 577-590, Springer-Verlag, Berlin, 1982.

Walter, H., *Ecology of Tropical and Subtropical Vegetation*. Oliver and Boyd, Edinburgh, 1971.

Walter, H., *Vegetation of the Earth and Ecological Systems of the Geobiosphere*, 2nd ed. Springer-Verlag, New York, 1979.

Warnant, P., L. Francois, D. Strivay, and J.-C. Gerard, CARAIB: A global model of terrestrial biological productivity, *Global Biogeochem. Cycles*, *8*(3), 255-270, 1994.

Wong, S.C., I.R. Cowan, and G.D. Farquhar, Stomatal conductance correlates with photosynthetic capacity, *Nature*, *282*, 424-426, 1979.

Woodward, F.I., *Climate and Plant Distribution*, Cambridge Univ. Press, New York, 1987

Woodward, F.I., T.M. Smith, and W.R. Emanuel, A global land primary productivity and phytogeography model, *Global Biogeochem. Cycles*, *9*(4), 471-490, 1995.

Zobler, L., A world soil file for global climate modeling, *NASA Tech. Memo.*, *87802*, 32 pp., 1986.

Alex Haxeltine and I. Colin Prentice, Global Systems Group, Department of Ecology, Lund University, Ecology Building, S-223 62 Lund, Sweden. (e-mail: alex@planteco.lu.se)

(Received January 17, 1996; revised July 8, 1996; accepted July 15, 1996.)